

Development of a cavitation erosion model

Matevž Dular^{a,b,*}, Bernd Stoffel^a, Brane Širok^b

^a Chair of Turbomachinery and Fluid Power, Darmstadt University of Technology, Magdalenenstr. 4, 64289 Darmstadt, Germany

^b Laboratory for Water and Turbine Machines, University of Ljubljana, Askerceva 6, 1000 Ljubljana, Slovenia

Received 14 December 2004; received in revised form 19 December 2005; accepted 24 January 2006

Available online 28 February 2006

Abstract

A study of visual and erosion effects of cavitation on simple single hydrofoil configurations in a cavitation tunnel was made. A thin copper foil, applied to the surface of the hydrofoils, was used as an erosion sensor. The cavitation phenomenon on hydrofoils at different flow conditions (system pressure, water gas content, flow velocity) was observed. Results that showed a significant relationship between cavitation erosion and the visual effects of cavitation made it possible to use these information to develop a cavitation erosion model. The model is based on the physical description of different phenomena (cavitation cloud implosion, pressure wave emission and its attenuation, micro-jet formation and finally pit formation), which are involved in the process of pit formation. It is capable to predict the influence of significant parameters as flow velocity and gas content of water.

The model that was developed on the basis of measurements of cavitation on a single hydrofoil was later tested on an actual hydraulic machine in the form of a radial pump. The predicted magnitude and distribution of cavitation damage relates well to the experimentally measured one.

© 2006 Elsevier B.V. All rights reserved.

Keywords: Cavitation; Damage; Computer-aided image processing; Erosion model

1. Introduction

The cavitation damage is caused when a bubble collapses in the vicinity of a solid surface. Since then a wide range of studies that deal with problems from bubble dynamics to material testing, have been made all aiming toward deeper understanding of the phenomena. The problem is a difficult one because it involves complicated flow phenomena combined with the reaction of the particular material of which the solid surface is made.

Recently there were many attempts to predict the magnitude of the cavitation erosion. For example Pereira et al. [1] found a relation between the volume of transient cavities and its rate of production to the material deformation energy. Fortes-Patella et al. [2] suggested that the damage of the solid surface is a consequence of a sequence of events – from cavitation cloud collapse to the spherical implosion of a single bubble that causes the damage. Present authors Dular et al. [3] and Širok et al. [4]

suggested that a strong correlation between erosion of the surface and visual cavitation structures exists. However an attempt to include the whole sequence of events, that lead to the appearance of damage on the surface, into a method of damage prediction, has not yet been successfully made.

Probably it is the so-called micro-jet phenomenon (Plesset and Chapmann [5], Lauterborn and Bolle [6]), which is responsible for the occurrence of initially microscopic damage (pits) of the solid surface. It was found that the liquid jet that penetrates the bubble can reach a velocity of several hundreds m/s.

The model gives a new option of cavitation erosion prediction and more importantly embraces the theories of cavitation cloud collapse (Shimada et al. [7], Brennen [8]), attenuation of the pressure wave (Beranek [9]), micro-jet formation (Plesset and Chapmann [5]) and finally pit formation (Lush [10]). The model was tested on results of recent experiments of Dular et al. [3,11] and Bachert et al. [12].

The paper firstly discusses the relation between optically observed cavitation structures on different single hydrofoils and the erosion on the surface of the hydrofoils. It gives a physical explanation of the processes involved in damage occurrence and of the influences of different flow parameters on the magnitude of damage. A proposal of a cavitation erosion model, which is

* Corresponding author. Tel.: +386 1 4771 453; fax: +386 1 2518 567.

E-mail addresses: matevz.dular@fs.uni-lj.si, matevz.dular@email.si (M. Dular), stoffel@tfa.maschinenbau.tu-darmstadt.de (B. Stoffel), brane.sirok@fs.uni-lj.si (B. Širok).

Nomenclature

A_{pit}	pit area
A_{ref}	reference area
A_{rel}	relative area
c	sonic velocity
d_{pit}	pit depth
f	shedding frequency
k_1	coefficient
k_2	coefficient
p	pressure
Δp	pressure difference
p_{def}	deformation pressure
p_y	yield stress
p_{∞}	free stream pressure
P	power
$P(\text{mj})$	probability of micro-jet
r_{jet}	jet radius
r_{pit}	pit radius
s	standard deviation of gay level
t	time
t_{def}	deformation time
v	velocity
v_{crit}	critical velocity
v_{def}	deformation velocity
v_{jet}	jet velocity
v_{ref}	referenced velocity
V	volume
x	distance of cloud implosion

Greek symbols

α	volume fraction
γ	nondimensional distance
κ	polytropic constant
μ	dynamic viscosity
ν	kinematic viscosity
ρ	density
σ	cavitation number
τ	time of exposure
ω	shock frequency

based on experimental studies of erosion and visual effects of cavitation on single hydrofoils, is given. The results of model prediction are compared to the experimental results of pitcount measurements on single hydrofoils and finally the model is tested on geometry similar to that of a real turbine machine – radial pump runner.

2. Experimental investigations

The experimental techniques were already discussed extensively in a previous paper from present authors (Dular et al. [3]). Cavitation tests were performed in a cavitation tunnel at the Laboratory for Turbomachinery and Fluid Power, Darmstadt University of Technology.

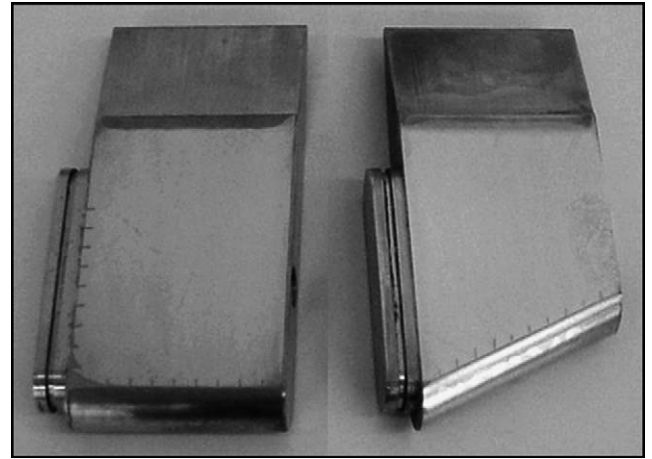


Fig. 1. Copper coated CLE and ALE hydrofoils used for the experiment. The hydrofoils are 107.9 mm long, 50 mm wide and 16 mm thick.

Two simple hydrofoils were used. The basic geometry is a 50 mm wide, 107.9 mm long symmetric hydrofoil with a circular leading edge and constant thickness of 16 mm, having a wedge shape near the trailing edge (CLE – Circular Leading Edge hydrofoil). In order to obtain three-dimensional cavitation effects the basic geometry was modified by sweeping back the leading edge at an angle 25° (ALE – Asymmetric Leading Edge hydrofoil) (Fig. 1).

The tested hydrofoil was put into a rectangular test section of the cavitation tunnel with closed circuit what enabled to vary the system pressure and consequently the cavitation number. The test section of the cavitation tunnel is 500 mm long, 100 mm high and 50 mm wide. Two observation windows are mounted for top and side view observation.

The velocity in the reference plane upstream of the hydrofoil was held constant at 13 m/s (Reynolds number based on hydrofoil length was: $Re = 1.4 \times 10^6$) except for two measurements at 10 and 16 m/s ($Re = 1.08 \times 10^6$ and 1.73×10^6 , respectively). Developed cavitating flow was observed at 5° incidence angle and at different values of cavitation number (2.5, 2.3, 2.0), which is defined as the difference between the pressure at the inlet to the test section p_{∞} (measured at the position 400 mm upstream of the hydrofoil) and vapour pressure p_v (at system temperature) divided by the dynamic pressure (defined by fluid density ρ and flow velocity v):

$$\sigma = \frac{p_{\infty} - p_v}{\rho v^2 / 2}. \quad (1)$$

Considering the combination of inaccuracies of pressure, velocity and temperature measurements, the cavitation number could be determined within ± 0.02 of global uncertainty.

Water quality, which can be measured by its content of dissolved and undissolved gasses ϕ , was controlled using the bubble generator system. For the majority of tests the gas content was kept at a minimum possible level – approximately $14.3 \pm 0.5 \text{ mg}_g/\text{l}_w$ (milligram of gas per liter of water). Additionally three measurements were made at higher water gas contents (25.9, 36.7 and 48.9 mg_g/l_w) to study the influence of this parameter on the aggressiveness of cavitation erosion.

Table 1
Parameters of tested cavitation conditions

Test	Hydrofoil	σ	v (m/s)	ϕ (mg _g /l _w)
1	CLE	2.0	13	14.0
2	CLE	2.3	13	13.8
3	CLE	2.5	13	14.0
4	CLE	2.3	13	36.7
5	CLE	2.3	13	25.9
6	CLE	2.3	13	48.9
7	CLE	2.3	10	13.9
8	CLE	2.3	16	13.8
9	ALE	2.0	13	14.8
10	ALE	2.3	13	14.7
11	ALE	2.5	13	14.7

The investigated cavitation conditions are presented in Table 1.

2.1. Cavitation image capturing

A CCD camera SensiCam with sensor CCD-Interline Progressive Scan was used. Images were captured at 8 bit resolution in m-jpeg format. The size of the captured image is 860 × 1280 pixels for the top view and 1280 × 860 pixels in case of the side view.

Results of visualization are presented for the case of ALE hydrofoil where the shedding is asymmetrical and therefore more illustrative than in for the case of CLE hydrofoil. Fig. 2 shows shedding of the cavitation structures on the ALE hydrofoil at low gas content and at a cavitation number $\sigma = 2.3$ from top view. Flow is from left to right. It is obvious that the cavitation zone is asymmetrical and that cavitation cloud separation occurs only in the region where the length of the hydrofoil is the shortest while it is steady on the other side.

Mean value and standard deviation of gray level in the images were calculated (50 images of each cavitation condition were used for statistical evaluation).

Results of statistically evaluated cavitation condition for ALE hydrofoil at a cavitation number $\sigma = 2.3$, flow velocity $v = 13$ m/s and low gas content $\phi = 14.7$ mg_g/l_w in Fig. 3. Left images represent the mean value (scaled to 0 – black, 250 – white) while the right ones represent standard deviation of gray

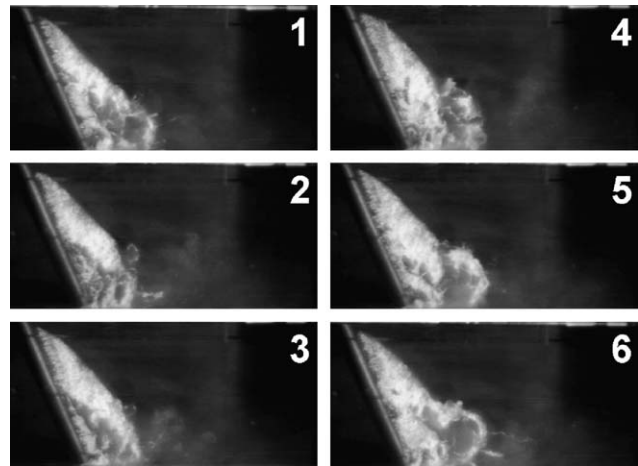


Fig. 2. Sequence of top view images for ALE hydrofoil. The flow is from left to right. The cavitation region is only partially unsteady – the cavitation cloud separation occurs only in the region where the length of the hydrofoil is the shortest.

level (scaled to 0 – white, 50 – black). The upper two images show the top view and the bottom two images show the side view.

If one compares Figs. 2 and 3 a distinctive relation between the region of cavitation cloud separation and the maximum of the standard deviation of gray level can be seen. The cloud separation occurs only in the region where the length of the hydrofoil is the shortest (Fig. 2) – we see that this region is characterised by higher values of standard deviation of gray level (Fig. 3).

2.2. Cavitation erosion tests

Due to the time limitation of the experiment only damage in the incubation period was studied (where damage is already present but there is no material loss).

To get the information about the erosion on the whole surface of the hydrofoil, a polished copper foil, 0.2 mm thick, was fixed to its surface using an adhesive film. The hardness of the copper coating was approximately 40 HV. A sufficient number of pits was obtained after 1 h exposure to the cavitating flow (the exposure time was constant for all operating conditions).

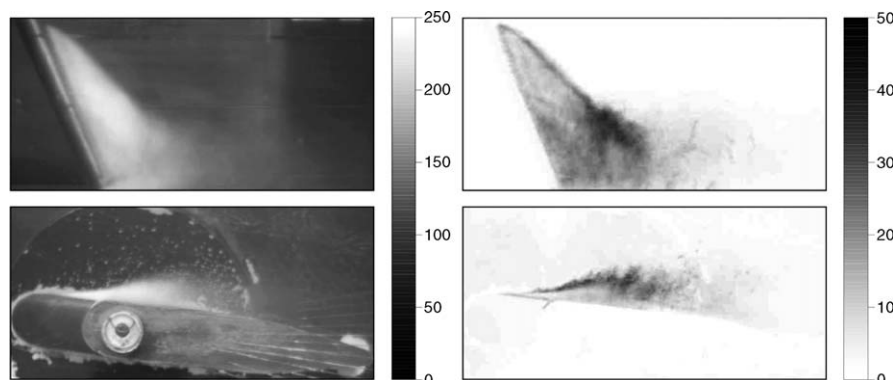


Fig. 3. Mean value and standard deviation for ALE hydrofoil; $\sigma = 2.3$, low gas content $\phi = 14.7$ mg_g/l_w. Standard deviation maximum reveals that the cloud separation occurs only in the region where the length of the hydrofoil is the shortest.

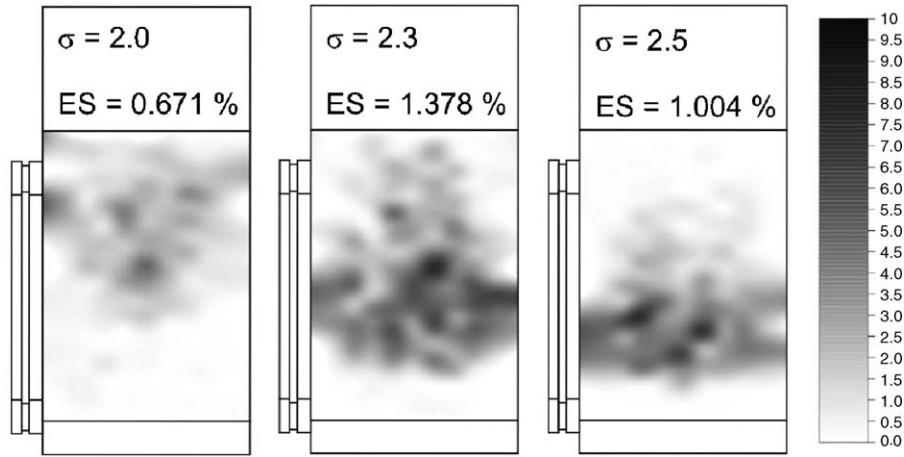


Fig. 4. Pit distribution for CLE hydrofoil, low gas content $\phi < 15 \text{ mg}_g/\text{l}_w$. The maximum of damage moves away from the leading edge as cavitation number decreases.

Pits have a diameter in order of magnitude 10^{-5} m , and can be distinguished only by sufficient magnification. Images of the pitted surface were acquired using an Olympus BX-40 microscope and a CCD camera.

The intensity of cavitation erosion was determined with the pit-count method (Dular et al. [3]). The method is based on the assumption that the area of the pitted surface and the number of pits that are created by bubble implosions (micro-jet impacts) in a certain time of exposure to cavitating flow give a quantitative measure of the intensity of cavitation erosion. The pit-count method gives a distribution of the number and the area of the pits and consequently the distribution of the magnitude of cavitation erosion on the surface.

Each contour diagram (Figs. 4–7) is a result of an interpolation of pit-count measurements at approximately 925 positions on the hydrofoil surface.

The flow is from bottom to top. The results of surface damage are scaled from 0% surface damage – white to 10% surface damage – black (in case of variable flow velocity the scale reaches to 12% surface damage). The value of eroded surface (ES) represents the part of the whole surface that is damaged (covered by pits).

Fig. 4 reveals that, as expected, the region of maximum cavitation damage moves away from the leading edge when cavitation number is decreased. Interestingly, the maximum value of total damaged surface (ES) occurs at cavitation number 2.3 and not at 2.0 as expected. The reason lies in the fact that the region of cloud separation lies downstream of the copper coated surface and also further away from the hydrofoil surface.

Fig. 5 confirms our hypothesis that the cavitation erosion is conditioned by the separation of cavitation clouds. The damaged surface is predominantly in the region near the edge where the length of the hydrofoil is the shortest – in the same region where unsteady cavitation (with cloud separation) is present.

Tests with variable flow velocity revealed an obvious relation between flow velocity and erosion rate. The cavitation is much more aggressive at higher flow velocities. The distribution of the pits and the position of the maximum magnitude of damage are similar for all the tests since cavitation number was held constant ($\sigma = 2.3$) – the topology of cavitation structures practically does not change when the gas content is altered. The reasons for the significant influence of flow velocity are given later in the paper.

One can see that erosive aggressiveness decreases significantly when the gas content rises. The surface sustains

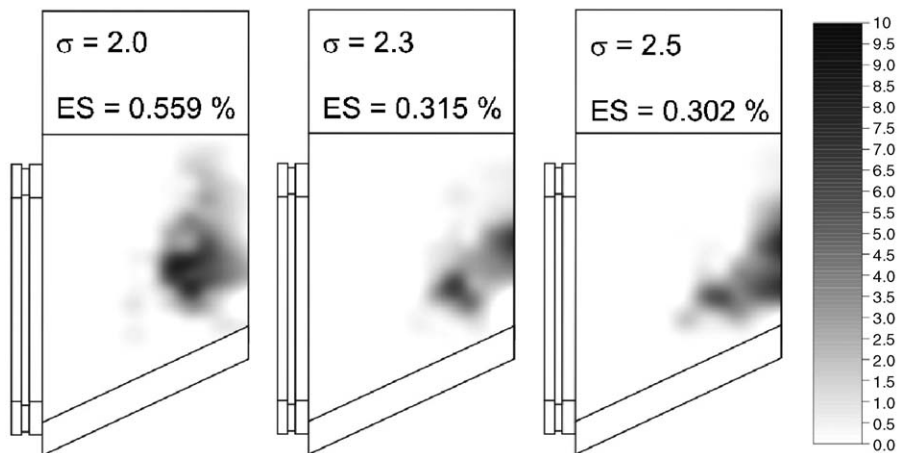


Fig. 5. Pit distribution for ALE hydrofoil, low gas content $\phi < 15 \text{ mg}_g/\text{l}_w$. The damage is concentrated in the region where the hydrofoil is the shortest.

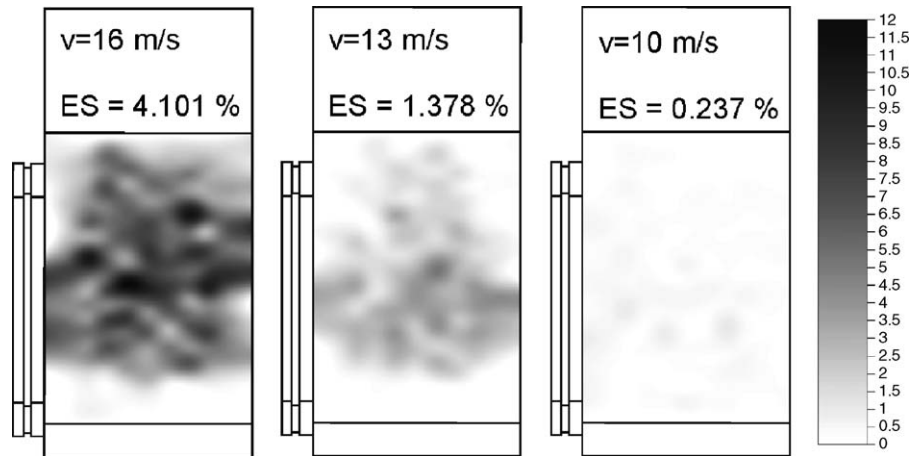


Fig. 6. Pit distribution for CLE hydrofoil, cavitation number 2.3, low gas content $\phi < 15 \text{ mg}_g/\text{l}_w$ and different flow velocities. The pit distribution remains almost the same while the magnitude increases dramatically when velocity is increased.

almost 50 times less damage in the case with high gas content ($\phi = 48.9 \text{ mg}_g/\text{l}_w$) than in cases with low gas content ($\phi = 13.8 \text{ mg}_g/\text{l}_w$). Similarly to the tests with variable flow velocity, the position of maximum erosion magnitude and the distribution of pits on the hydrofoil remain almost constant for all the cases, since the cavitation number was constant. The reasons for the significant influence of gas content of water are discussed later in the paper.

The previous study (Dular et al. [3]) showed that the magnitude of cavitation damage is correlated with unsteadiness of cavitation structures. For example, the effect can be seen if we compare Figs. 2, 3 and 5 (middle hydrofoil – $\sigma = 2.3$). Fig. 2 shows a sequence of cavitation images on ALE hydrofoil. Statistical evaluation reveals that the standard deviation has its maximum in the region where cavitation cloud separation occurs (in the region where the hydrofoil length is the shortest). It is obvious (from Fig. 5 – middle hydrofoil – $\sigma = 2.3$) that most of the damage also occurs in this region. Results point out that the standard deviation of gray level is a variable that could be included in a cavitation erosion model as a measure of unsteadiness, which is indirectly linked to the magnitude of cavitation erosion.

3. Theoretical model

A successful prediction of cavitation erosion still remains one of the big goals in this field of research. As shown above one could use visualization techniques as an input for cavitation erosion model to determine the region and possibly the magnitude of cavitation damage.

The process of pit formation is very complex. The presented theory explains the pit formation in the following way (Fig. 8):

- Collapse of the cavitation cloud causes a shock wave that spreads in the fluid.
- The magnitude of the shock wave is attenuated as it travels toward the solid surface.
- Single bubbles are present near the solid surface. As the shock wave reaches them, they begin to oscillate and a micro-jet phenomenon can occur.
- The damage (single pit) is caused by high velocity liquid jet impact to the solid surface.

If we take into account only the incubation period (surface is plastically deformed but no material loss is present) we can

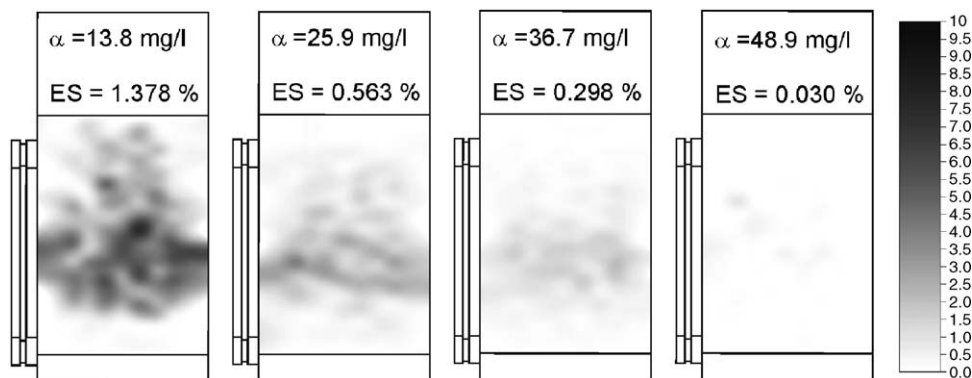


Fig. 7. Pit distribution for CLE hydrofoil, cavitation number 2.3, flow velocity 13 m/s, at different gas content ϕ . While the aggressiveness of erosion decreases when gas content is increased, the pit distribution remains almost the same.

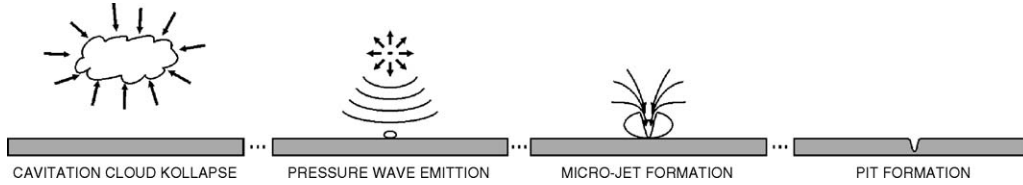


Fig. 8. The events that are included in cavitation damage occurrence are: bubble cloud implosion, pressure wave emission and its attenuation, formation of micro-jet and finally pit formation.

say that the eroded surface of a submerged body is a result of repetition of abovementioned processes.

Influence of flow velocity and presence of gas in the water on cavitation aggressiveness also have to be considered. Each of the processes is more thoroughly discussed.

3.1. Amplitude of the emitted pressure wave

The power and consequently the magnitude of the emitted pressure wave are closely related to the velocity of the change of the vapour cloud volume (velocity of cavitation cloud collapse) and to the surrounding pressure (Fortes-Patella et al. [2]). We can write the following relation:

$$P_{\text{wave}} = \Delta p \left(\frac{dV}{dt} \right), \quad (2)$$

where Δp is the difference between the surrounding pressure and vapour pressure ($p_{\text{sur}} - p_v$) and dV/dt is the change of the vapour cloud volume in time t .

From the acoustics the magnitude of the emitted pressure wave is proportional to the square root of its power ($p_0 \propto \sqrt{P_{\text{wave}}}$). If we consider the surrounding pressure p_{sur} to remain approximately constant at an average level $\bar{p} = p_{\infty}/2$ (and $\Delta \bar{p} = \bar{p} - p_v$), we can write that the distribution of the mean change in cavitation cloud volume on the hydrofoil reveals the mean distribution of amplitude of the pressure wave that is emitted by the cavitation cloud collapse.

Since we have no possibility of measuring the instantaneous change of the cavitation cloud volume (the image capturing frequency was much lower than the frequency of vapour cloud shedding) a standard deviation of gray level s was used as the parameter, which is related to the power of the emitted pressure wave. Standard deviation can be used in this manner since it is a function of the change of the gray level in the image, which is a function of the cavitation cloud volume:

$$\text{gray level} = f(V) \Rightarrow s \propto \left(\frac{dV}{dt} \right). \quad (3)$$

The hypothesis is that the relation between the time derivative of vapour cloud volume and the distributions of standard deviation of gray level from side and top view exists. A possible measure of the emitted pressure wave power P_{wave} can be formulated in the following way:

$$P_{\text{wave}}(n, l) \propto \Delta \bar{p} \xi(n, l) = \Delta \bar{p} \left[\left(\frac{1}{M} \sum_m^M s_m \right) s_n \right]_{l=\text{const.}}, \quad (4)$$

where $\Delta \bar{p}$ is the mean pressure difference, M the height of the matrix, l, m and n are direction vectors and s_m and s_n are standard deviations of gray level in distribution matrix of side and top view, respectively (Fig. 9).

This way we get a parameter ξ that is related to the rate of the change in the cavity volume and together with $\Delta \bar{p}$ and a specific function f (that has to be determined iteratively) to the power of the cavitation cloud implosion pressure wave:

$$P_{\text{wave}}(n, l) = \Delta \bar{p} f(\xi(n, l)) \quad (5)$$

It was found that a linear function shows the best correlation to the experimental results (the relation was obtained by comparison of model predictions and results of experimental measurements from Hofmann [13]):

$$P_{\text{wave}}(n, l) = \Delta \bar{p} k_1 \xi(n, l) \quad (6)$$

A linear function is also used for the amplitude of the emitted pressure wave (the determination of the coefficients is explained in Section 4):

$$p_0(n, l) = k_2 \sqrt{P_{\text{wave}}} = \sqrt{k_1 k_2} \sqrt{\Delta \bar{p} \xi(n, l)}. \quad (7)$$

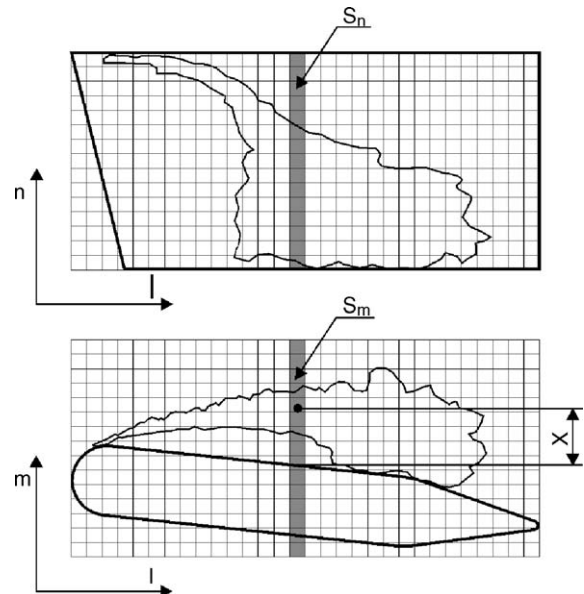


Fig. 9. The distribution of standard deviation of gray level in the coordinate system. Each cell contributes to the parameter ξ in Eqs. (4) and (5).

3.2. Distance of the cloud implosion from the hydrofoil surface

The position of the cloud collapse and consequently the distance of cloud collapse from the hydrofoil surface x can be determined from the standard deviation of gray level from the side view (Fig. 9). An equilibrium function was used:

$$x(l) = \frac{\sum_m^M (s_m m)}{\sum_m^M s_m} - m_h, \quad (8)$$

where m_h is the position of the hydrofoil surface at a specified l . The distance of cloud implosion had to be considered constant for each value of l , what represents a considerable simplification especially for the cases with asymmetrical hydrofoils.

3.3. Attenuation of the pressure wave

As the pressure wave travels away from its source its energy is gradually converted into heat. For our problem the main energy loss mechanism are the viscous losses generated from the friction within the fluid itself (Beranek [9]).

According to general acoustic theory we can determine pressure wave amplitude at a given distance x from the source with:

$$p = p_0 e^{-(2/3)(\omega^2/\rho_0 c^3)\mu x}, \quad (9)$$

where ω is the pressure wave frequency, μ the viscosity and c is the sonic velocity. μ and c are functions of the local vapour volume fraction α , which is calculated from the initial water gas content ϕ (Table 1).

3.4. Formation of micro-jet

Presence of a solid surface can influence the bubble collapse process so that it becomes asymmetrical. A well know theory developed by Plesset and Chapmann [5] determines the jet velocity which is:

$$v_{\text{jet}} = 8.97\gamma^2 \sqrt{\frac{p - p_v}{\rho}}, \quad (10)$$

where γ is the nondimensional distance of the bubble centre from the surface ($\gamma = H/R$, where H is the distance and R the bubble radius).

3.5. Pit formation

3.5.1. General aspects

The water hammer stress applied to the material at the impact of the liquid micro-jet can be considered as the main mechanism of damage to the solid surface (Plesset and Chapmann [5]). If the density and the sonic velocity of the solid are high compared to the density and the sonic velocity of the liquid, it is defined as:

$$p \approx v_{\text{jet}} \rho_0 c_0, \quad (11)$$

where ρ_0 , c_0 , are the density and the sonic velocity of liquid.

In the present approach the surface responds as a perfectly rigid solid until a certain compressive stress is reached and then behaves as a perfectly plastic solid, for which the stress will remain constant. The deformation only occurs if the water hammer pressure is higher than the limit pressure at which the plastic flow of the material occurs. This velocity, at which the stress high enough to produce a plastic flow of the material p_y is reached, was derived by Lush [10] and reads:

$$v_{\text{crit}} = \sqrt{\frac{p_y}{\rho_l} \left(1 - \left(1 + \frac{p_y}{B} \right)^{-(1/n)} \right)}, \quad (12)$$

where p_y is the yield stress of the material, $B = 301$ MPa and $n \approx 7.15$.

A part of the water hammer pressure wave (Eq. (11)) energy is needed to reach the plastic flow condition of the material. The rest of the pressure p_{def} is converted into deformation energy.

$$p_{\text{def}} \approx v_{\text{def}} \rho c = (v_{\text{jet}} - v_{\text{crit}}) \rho c. \quad (13)$$

The duration of the water hammer stress is as long as the time for the impact signal to traverse the radius of the jet (r_{jet}):

$$t_{\text{def}} = \frac{r_{\text{jet}}}{c}. \quad (14)$$

After that time a stagnation pressure $(1/2)\rho v^2$ is established. It is unlikely that any damage occurs in this period since the stagnation pressure is an order of magnitude smaller than the water hammer pressure (unless exceptionally high impact velocities are encountered).

If we consider only the centre of the impact where only motion (plastic flow) normal to the surface is present the maximum depth of the pit can be calculated:

$$d_{\text{pit}} = v_{\text{def}} t_{\text{def}}. \quad (15)$$

3.5.2. Pit geometry

The ratio between the pit radius and pit depth is not constant. Previous investigations showed that it usually lies between 15 and 30 but can also be as low as 2 and as high as 500 (Fortes-Patella et al. [14]). The mean ratio between the pit radius and pit depth (26.7) was determined from the laser profilometry measurements of the pitted surface of a copper specimen from the hydrofoil from the same cavitation tunnel done at LEGI – Grenoble (Reboud et al. [15]). Hence the pit radius is defined as:

$$r_{\text{pit}} = 26.7 d_{\text{pit}}. \quad (16)$$

The area of the pit seen normal to the material surface is then:

$$A_{\text{pit}} = \pi r_{\text{pit}}^2. \quad (17)$$

The measure of the damage caused by cavitating flow (the part of the damaged surface after a certain amount of time τ) can now be written:

$$A_{\text{rel}} = \frac{A_{\text{pit}} \tau f P(\text{mj})}{A_{\text{ref}}}, \quad (18)$$

where τ is the duration of the exposition to the cavitating flow, f the frequency of cavitation cloud implosion, $P(\text{mj})$ the probability of micro-jet occurrence and A_{ref} is the reference area.

The Eq. (18) is only valid in the incubation period of cavitation erosion where no mass loss is present.

3.6. Influences of fluid properties

Experimental results show obvious influences of fluid properties on cavitation erosion. It was shown that when the experiment was conducted in water with high gas content cavitation erosion was less aggressive. The main reason lies in the fact that the sonic velocity is lower in water with high gas content. Consequently compressibility and pressure wave attenuation are higher.

The sonic velocity of water considering the presence of gases is given by (Brennen [8]):

$$c = \left[(\rho_l(1 - \alpha) + \rho_g\alpha) \left(\frac{\alpha}{\kappa \bar{p}} + \frac{1 - \alpha}{\rho_l c_1^2} \right) \right]^{-1/2}, \quad (19)$$

where ρ_l and ρ_g are the density of the liquid and gas, respectively, α is the gas volume fraction and κ the polytropic constant of the gas.

The density and viscosity of the water considering the presence of gases are:

$$\rho = \alpha \rho_g + (1 - \alpha) \rho_l \quad (20)$$

and

$$\nu = \alpha \nu_g + (1 - \alpha) \nu_l. \quad (21)$$

3.7. Influences of flow velocity

Previous investigations (Dular et al. [11], Bachert [12] and Knapp et al. [16]) have shown that the flow velocity has an enormous influence on the aggressiveness of cavitation. A power law with coefficient $n = 5-8$ was found. Here we state some physical explanations of the velocity influence that are included in the cavitation erosion model.

- When the cavitation number is constant the pressure difference has to increase with the power of 2 when velocity is increased. This means that the pressure emitted at bubble cloud collapse will also rise with the power of 2. If a reference pressure \bar{p}_{ref} is used for the mean surrounding pressure \bar{p} an additional term must be introduced into the Eq. (7):

$$p_0(n, l) = \sqrt{k_1 k_2} \sqrt{\Delta \bar{p}_{ref} \xi(n, l) \left(\frac{v}{v_{ref}} \right)^2} \quad (22)$$

- When the cavitation number is constant the pressure difference has to increase with the power of 2 when the flow velocity is increased. Higher system pressure acts on the compressibility of the fluid. Observing Eq. (19) we can see that the sonic velocity c will be higher when the velocity and consequently the pressure is increased. The pressure p in equation Eq. (19) must then be defined as:

$$\bar{p} = \bar{p}_{ref} \left(\frac{v}{v_{ref}} \right)^2 \quad (23)$$

Past experiments have shown that the cavitation cloud shedding frequency will rise with the power of 2 when the flow velocity is increased (Böhm [17]). This results in more cavitation cloud collapses and consequently more shock waves, micro-jet impacts and finally pits. Eq. (18) needs to be corrected by adding another term:

$$A_{rel} = \frac{A_{pit} \tau f P(mj)}{A_{ref}} \left(\frac{v}{v_{ref}} \right)^2 \quad (24)$$

- There is a finite number of bubbles that have a potential to form a micro-jet in the flow. Since the time of bubble implosion (a few μ s) is much smaller than the time needed for transition of a bubble through the control volume (a few ms) the probability for a bubble to implode in micro-jet form does not alter with velocity (this hypothesis was also confirmed by past experiments, for example Knapp et al. [16] speaks of probability $P(mj) = 1/30,000$). Hence when the velocity is increased, more bubbles implode in the form of micro-jet in a certain time period. Therefore, an additional term is added to already modified Eq. (18) (Eq. (24)):

$$A_{rel} = \frac{A_{pit} \tau f P(mj)}{A_{ref}} \left(\frac{v}{v_{ref}} \right)^2 \left(\frac{v}{v_{ref}} \right) \quad (25)$$

4. Results – single hydrofoils

Setting up the problem needs a lot of iterative work. The coefficients k_1 and k_2 that are included in Eq. (7) and the liquid jet radius r_{jet} that is included in Eq. (14) were determined iteratively. Some guide lines about the values of the parameters can be found in past studies of Plesset and Chapman [5], Shimada et al. [7], Brennen [8], Lush [10] and Hofmann [13]. It is known that the cavitation cloud implosion emits a shock wave of magnitude of several MPa. The shock wave magnitude at its origin has not yet been experimentally determined because of the effect of attenuation, but theoretical work of Shimada et al. [7] and Brennen [8] set it in an order of 6 MPa. Some help was also gained from experimental measurements of the shock waves on similar geometries from Hofmann [13]. The coefficients k_1 and k_2 were chosen to fulfil the physical considerations of the shock wave magnitude – eventually a value $\sqrt{k_1 k_2} = 260$ was chosen.

A similar problem occurs when the radius of micro-jet is in question. Considering the theoretical works from Plesset and Chapman [5] and experimental results of Lauterborn and Bolle [6] and in addition the results of studies of the damaged surfaces, a value of $r_{jet} = 10 \mu$ m, was chosen as the most probable value for the average radius of the micro-jet.

A value of $\gamma = 1.1$ for the nondimensional distance of the bubble from the solid surface in Eq. (10) was chosen on the basis of a combination of theoretical and experimental results.

The values of densities and viscosities of water and water vapour ($\rho_l, \rho_v, \nu_l, \nu_v$) and the sonic velocity (c_l) and water vapour pressure (p_v) correspond to the ambient temperature of 20 °C.

The frequency of the pressure wave that is emitted by cavitation cloud collapse was found to lie between 0.5 and 1.7 MHz (Shimada et al. [7], Lohrberg [18]). A value of $f = 0.75$ MHz was chosen on the basis of theoretical studies and also based on

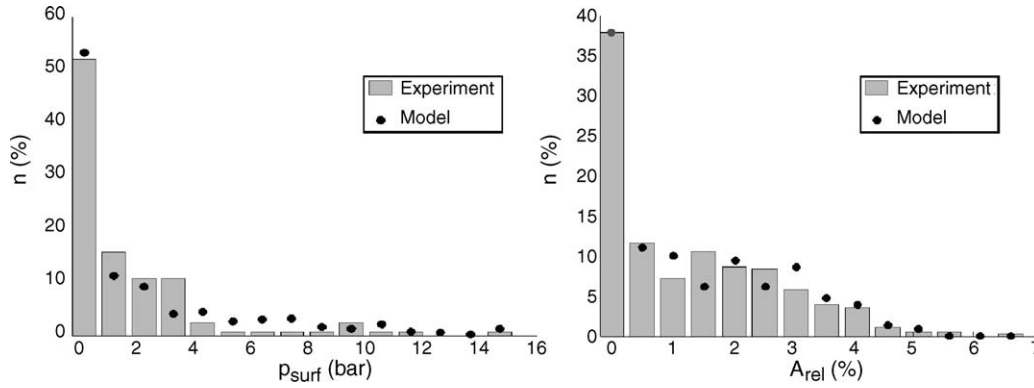


Fig. 10. Histograms of experimentally measured and predicted pressure on the surface of the hydrofoil (left) and local relative damaged surface (right). In both cases the model prediction relates very well to the experimental measurements.

measurements of pressure waves on similar geometries done by Hofmann [13].

Since the local gas volume fraction α was not a subject of measurements, it was estimated that (right after the cloud collapse) it is in the same order as the volume fraction of the initial gas content of the water ϕ (Table 1). Hence the parameter α (used for determining the fluid properties – Section 3.6) was calculated using:

$$\alpha = \frac{\phi}{\rho_g}, \tag{26}$$

where ϕ is in kg_g/m_w^3 and ρ_g is gas density. Since the majority of the gas in the water is air, a value $\rho_g = 1.225 \text{ kg}/\text{m}^3$ was used. The values from $\alpha \approx 0.01$ for low gas content to $\alpha \approx 0.04$ for high gas content relate well to the results of experimental measurements of void fraction within cavitation by Stutz and Reboud [19].

The yield stress p_y of the foil made of pure copper (99.9%) is $p_y = 200 \text{ MPa}$.

The values of flow velocity v , system pressure p_∞ and shedding frequencies f were acquired during experiment.

It is possible to compare intermediate results of experimental measurements and model prediction on CLE geometry at a

cavitation number 2.3, flow velocity 13 m/s and low gas content $\phi = 13.8 \text{ mg}_g/\text{l}_w$.

The left diagram in Fig. 10 represents the distributions of values of the measured (Hofmann [13]) and predicted dynamic pressure on the surface of the hydrofoil. n represents the frequency of occurrence of a state with a specific pressure range p_{surf} . The model prediction is plausible and one can conclude that it correctly predicts that the surface sustains few pressure peaks with amplitude high enough to trigger the process of pit creation.

Similarly the right diagram represents the frequency of occurrence of a specific rate of damage A_{rel} on the surface. In this case also, the model correctly predicts that the majority of the hydrofoils surface sustains little damage and that only few specific regions are severely damaged.

The model was used for prediction of surface damage caused by cavitation on two different hydrofoils. The diagrams have the same form as the experimental ones (Figs. 4–7).

We see that the predicted surface damage for the CLE hydrofoil relates very well to the experimental results (comparing Figs. 4 and 11). If we compare model prediction and experimental measurements for the case of cavitation number 2.0, we see that the model predicts the damage to be concentrated

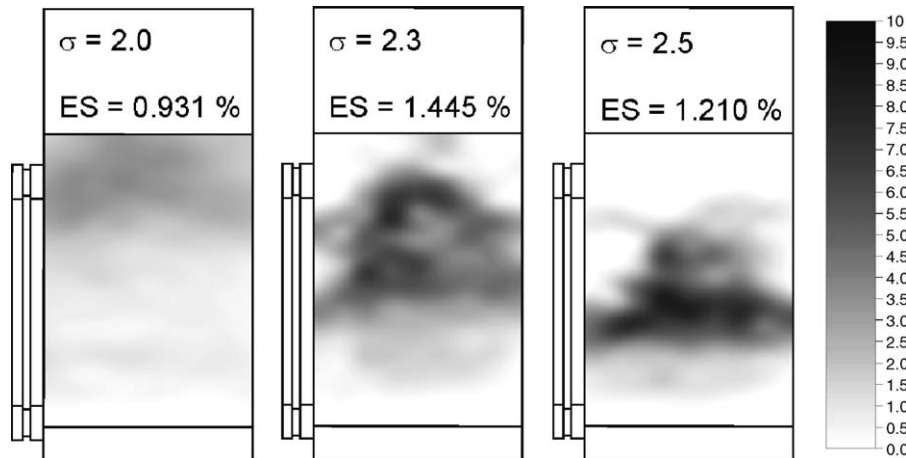


Fig. 11. Predictions of pit distributions for CLE hydrofoil at low gas content ($\phi < 15 \text{ mg}_g/\text{l}_w$), constant flow velocity ($v = 13 \text{ m/s}$) and different cavitation numbers. Observing Fig. 4, a very good correlation between measurements and prediction can be seen.

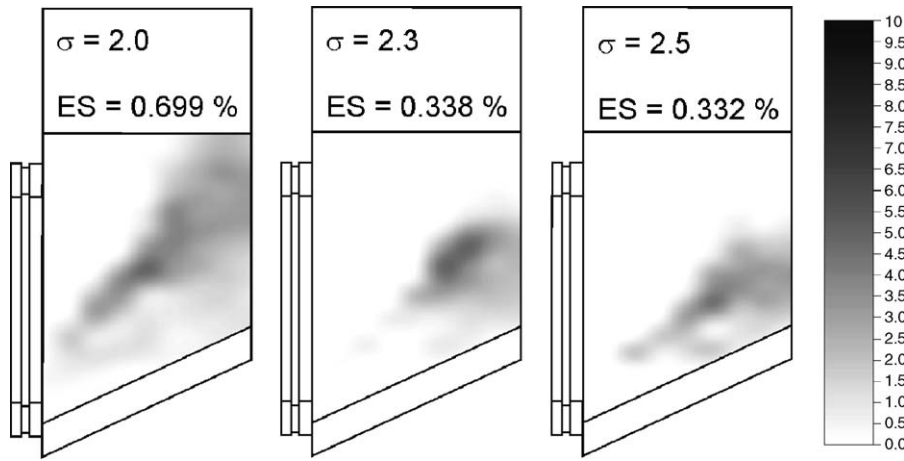


Fig. 12. The prediction of damage distribution for ALE hydrofoil at low gas content ($\phi < 15 \text{ mg}_g/\text{l}_w$), constant flow velocity ($v = 13 \text{ m/s}$) and different cavitation numbers. As in experiments, the pits are concentrated in a cluster in the region where the length of the hydrofoil is the shortest.

in the region near the end of the plane part of the hydrofoil, while the experimentally measured damage stretches towards the leading edge and is not so concentrated. The predicted distributions at cavitation numbers 2.3 and 2.5 relate even better to the experimental results. The model also correctly predicts the cavitation at cavitation number $\sigma = 2.3$ to be the most aggressive one (observing the ES values and also top diagram in Fig. 15).

As a consequence of the hypothesis that cavitation damage is conditioned by cavitation cloud separation (which is characterised by higher values of standard deviation of gray level), the model correctly predicts the damage to occur predominantly in the region where the hydrofoil length is the shortest, for ALE hydrofoil (Fig. 12). The predicted damage is somewhat more evenly distributed over the hydrofoil than experiments have shown (comparing Figs. 5 and 12). The model wrongly predicts a significant stretch of damage reaching from the “main damage cluster” toward the region where the hydrofoil length is the longest. The stretch cannot be seen in experimental results (Fig. 5) and is a result of small oscillations of quasi-steady cavitation in this region that contribute to higher values of standard deviation of gray level (seen also in standard deviation diagram

in Fig. 3) but have nothing to do with cloud separation (see also Dular et al. [3]).

The capability of the model to predict the influence of flow velocity was tested.

We can see that the model correctly predicts a significant decrease of aggressiveness of cavitation when the flow velocity is decreased (Fig. 13). As in the experiment (Fig. 6) the distributions remain almost the same for all flow velocities, since the topology of the cavitation structures remains almost the same.

Finally the ability of the model to predict the influence of water gas contents was put in question.

The diagrams in Fig. 14 show that the model responds very well to the change of water gas content. When the gas content increases the aggressiveness decreases dramatically. Again the distribution of the damage along the hydrofoils remains approximately the same, as the topology of the cavitation structures does not change significantly when the gas content is changed.

Integral experimental and predicted (ES – relative eroded surface) values were compared (Fig. 15).

The prediction of relative eroded surface (ES parameter) is very good (Fig. 15). One can see that the model always correctly

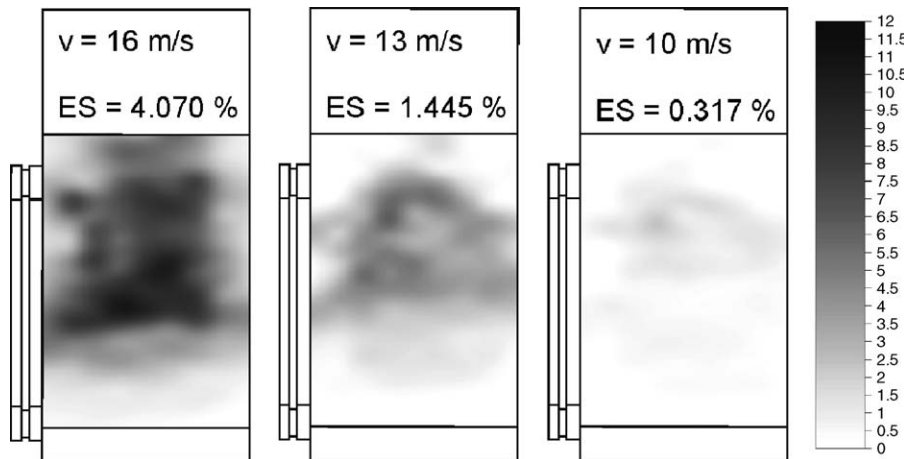


Fig. 13. The prediction of damage distribution for CLE hydrofoil at low gas content ($\phi < 15 \text{ mg}_g/\text{l}_w$), cavitation number $\sigma = 2.3$ and variable flow velocity ($v = 10, 13$ and 16 m/s). An obvious decrease of cavitation aggressiveness when flow velocity is decreased is correctly predicted.

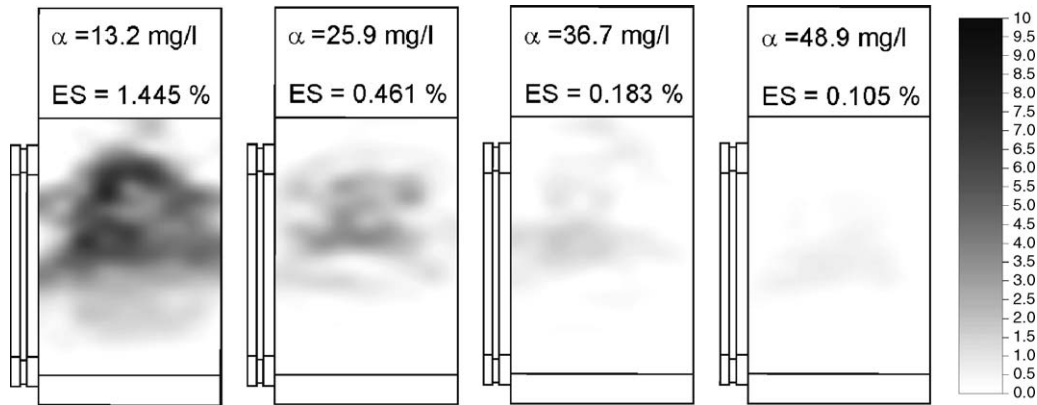


Fig. 14. The prediction of damage distribution for CLE hydrofoil at constant flow velocity ($v = 13$ m/s), cavitation number $\sigma = 2.3$ and variable gas content ϕ . Model correctly predicts the decrease of damage when the gas content is increased.

predicts the trend of damage (ES parameter) versus cavitation number, although discrepancies exist. The model is, for example, also capable of predicting the maximum damage at cavitation number $\sigma = 2.3$ for the CLE hydrofoil what was also found during experimental measurements.

The diagrams in Fig. 16 show the influence of flow velocity and water gas content on the aggressiveness of cavitation.

Influence of flow velocity on parameter ES (relative eroded surface) can be seen in top diagram in Fig. 16. A significant exponent relationship was found during experiments. Previous

investigations (Knapp et al. [16]) derived an empirical relation:

$$\frac{ES_1}{ES_2} = \left(\frac{v_1}{v_2}\right)^n; \quad n = 5, \dots, 8 \quad (27)$$

Present study sets the exponent to $n = 6.1$. The model prediction slightly underestimates the influence of the flow velocity and sets the exponent to $n = 5.5$.

The bottom diagram in Fig. 16 shows the influence of water gas content on ES parameter. The model firstly (at low gas contents) somewhat overestimates and later (at higher gas contents) slightly underestimates the influence of water gas content. Nevertheless the model prediction shows the correct trend.

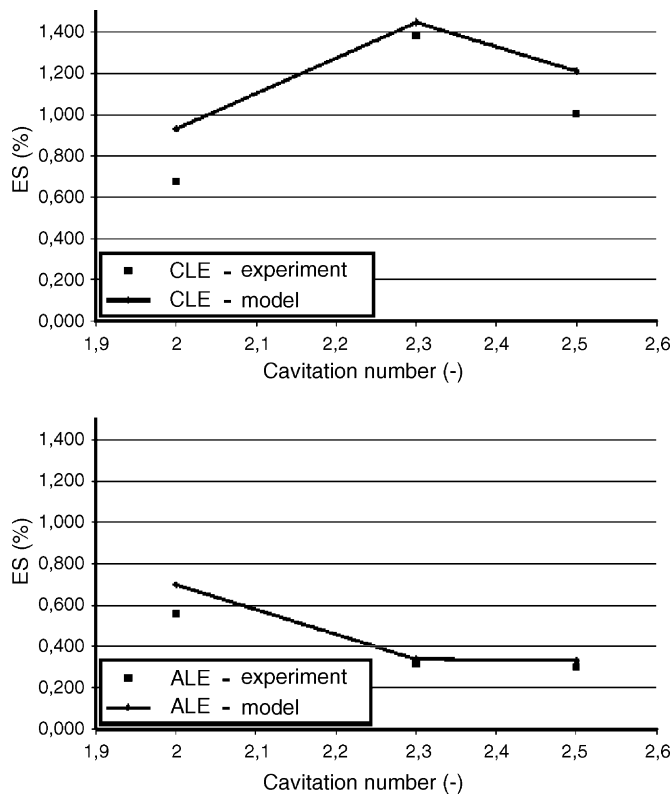


Fig. 15. Experimentally measured and predicted integral parameter of damage (relative eroded surface – ES) for CLE (top) and ALE (bottom) hydrofoil at different cavitation numbers and constant velocity ($v = 13$ m/s) and gas content ($\phi < 15$ mg_g/l_w).

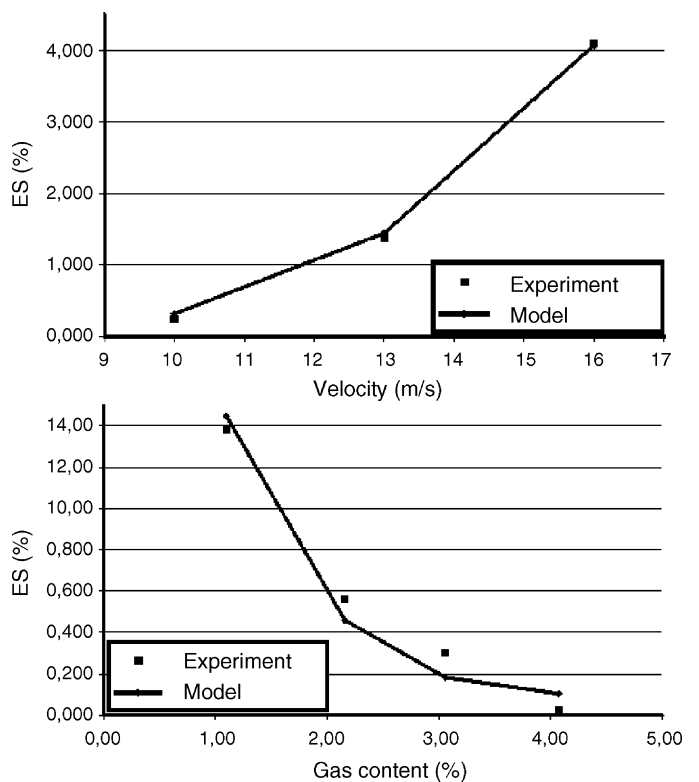


Fig. 16. Experimentally measured and predicted ES parameter for CLE hydrofoil at a constant cavitation number ($\sigma = 2.3$) and variable flow velocity (top) and variable gas content (bottom).

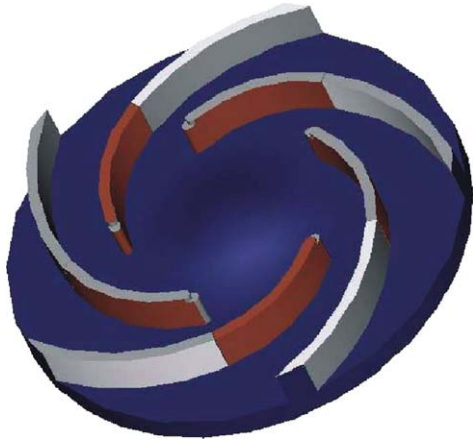


Fig. 17. Radial pump impeller with two dimensionally curved blades. Detachable part of the blades (front darker part) on which copper foil was mounted can be seen.

5. Results – radial pump

The model that was developed on the basis of measurements on single hydrofoils was additional tested on a radial pump geometry (Fig. 17). A special radial pump with two-dimensional blade geometry was manufactured. Its specific speed is $n_q = 18 \text{ min}^{-1}$, the blade channels are 23 mm wide, the nominal flow rate is $Q = 209 \text{ m}^3/\text{h}$ and the nominal rotation speed is $n = 2160 \text{ min}^{-1}$. The shroud of the impeller and parts of the pump casing are made of acrylic glass what enables observation of cavitation in the impeller. The blades can be removed from the pump so that the damage on the surface can be evaluated.

The experimental techniques used are exactly the same as in the case of single hydrofoils. A thin copper foil that was attached to the blades was used as damage sensor. Pit-count technique was employed to determine the surface damage. The radial pump test rig only allows recording of the cavitation from side view so the images of cavitation were recorded only from this direction. Special care was given to the illumination since the image properties greatly depend on it. The illumination and camera position was adjusted until the images of the same quality and spectrum as for the case of single hydrofoils were recorded. Recorded images were again statistically evaluated – the standard deviation of the gray level was calculated.

The parameters of five different cavitation conditions that were tested are presented in Table 2. The tests were carried out at five operating points at overload conditions (i.e. cavitation

Table 2
Tested operating points for the radial pump

Operating point	Flow rate, q (%)	Cavitation number
(a)	97.0	0.264
(b)	99.4	0.275
(c)	101.3	0.302
(d)	102.5	0.313
(e)	104.5	0.552

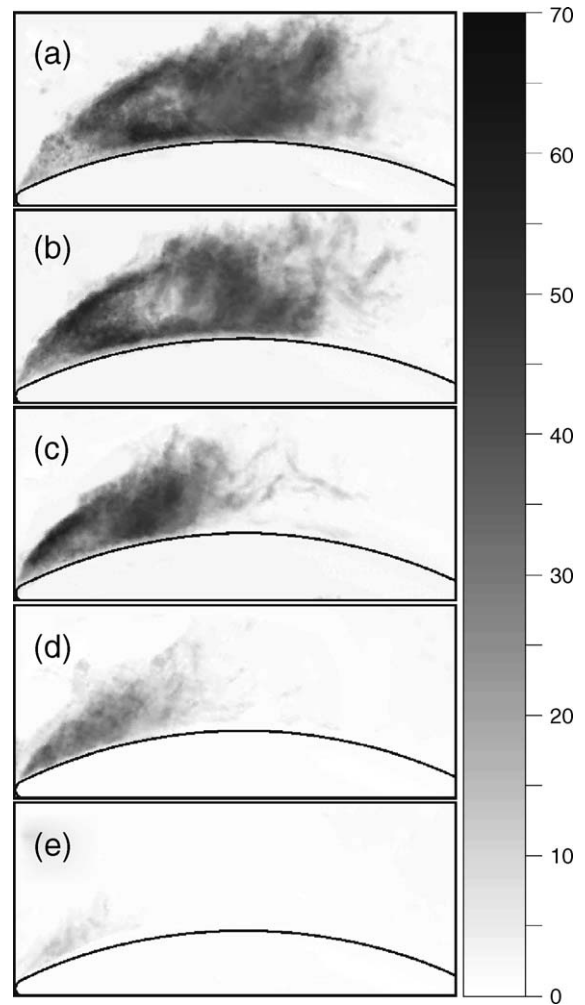


Fig. 18. Distributions of standard deviation of gray level for five operating conditions (a–e). A significant decrease in the value of standard deviation can be seen as cavitation number is increased (moving from (a) to (e)).

is present on pressure side). The gas content of water ϕ was held approximately constant at $28 \pm 0.6 \text{ mg}_g/\text{l}_w$ for all operating points.

The results of visualization for the five operating points (a–e) can be seen in Fig. 18.

Distributions of the standard deviation of gray level for the five operating points are shown in Fig. 18. The impeller rotates counter-clockwise. The results are scaled from 0 – white to 70 – black. It can be seen that the standard deviation of the gray level falls when we move from point (a) to (e) (when the cavitation number increases). The fluctuating zone (zone of cavitation cloud separation) characterised by higher values of standard deviation moves further away from the blade leading edge (left side of the images) when the cavitation number is decreased (from point (e) to point (a)). Similar to the results of measurements on single hydrofoil geometries the damage was mainly detected in the region where higher values of standard deviation of gray level were found.

Since we have visual information only from one point of view the function ξ of the cavitation model (Eq. (4)) had to be

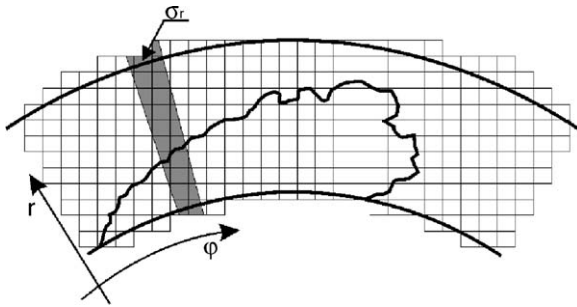


Fig. 19. The matrix of standard deviation of gray level was treated in the polar coordinate system. The pit distribution could only be modelled in φ (or l) direction.

modified so that the modified equation reads:

$$P_{\text{wave}}(\varphi) \propto \Delta \bar{p} \xi(\varphi) = \Delta \bar{p} \left[\left(\frac{1}{R} \sum_r^R s_r \right) s_r \right]_{\varphi=\text{const.}} \quad (28)$$

Fig. 19 shows how the standard deviation matrix is treated in the polar coordinate system. The principle used for post-processing of already statistically evaluated visual data is generally the same (apart from different coordinate system) as the one used for single hydrofoils. Since no top view images were available only the information about damage distribution in φ direction (or as a function of distance from blade leading edge l) could be modelled.

The results of experimental measurements and model prediction can be seen in Fig. 20. Damage was always measured on the whole surface of two blades that were mounted in the pump impeller. The presented experimental results were obtained by averaging the pit-count data for each distance from the leading edge l on the whole blade surface for two blades for each

operating point:

$$A_{\text{rel}}(l) = \frac{1}{2} \left[\left(\frac{1}{D} \sum_d^D A_{\text{rel}}(d, l) \right)_{\text{BLADE}_1} + \left(\frac{1}{D} \sum_d^D A_{\text{rel}}(d, l) \right)_{\text{BLADE}_2} \right], \quad (29)$$

where d is the coordinate in blade width direction; D the width of the blade (23 mm).

In general the model prediction agrees well with experimental measurements. The position and magnitude of the damage is well predicted in (b), (c) and (d) cases. In case (a) a shift between the experimental and predicted results exists – the model predicts the maximum of damage to occur nearer (about 15 mm) to the leading edge. In case (e) no damage was found either by measurements or with model prediction.

6. Conclusions

Erosion on single hydrofoils and its relationship to visual cavitation structures was studied. It was found that the value of standard deviation of gray level could be used as the parameter for describing the unsteadiness of cavitation and that this parameter could be used as an input for the cavitation erosion model. Experiments confirmed the hypothesis that the cavitation erosion is conditioned by the cavitation cloud separation. Effects of parameters as the flow velocity and the water gas content were also studied and physical explanations were given. A well-known power law that relates the cavitation aggressiveness to the flow velocity was confirmed. The explanation lies in the facts that the pressure raises, the cavitation shedding frequency increases and the bubble number density increases in time. The decrease of the aggressiveness due to the increase of the water

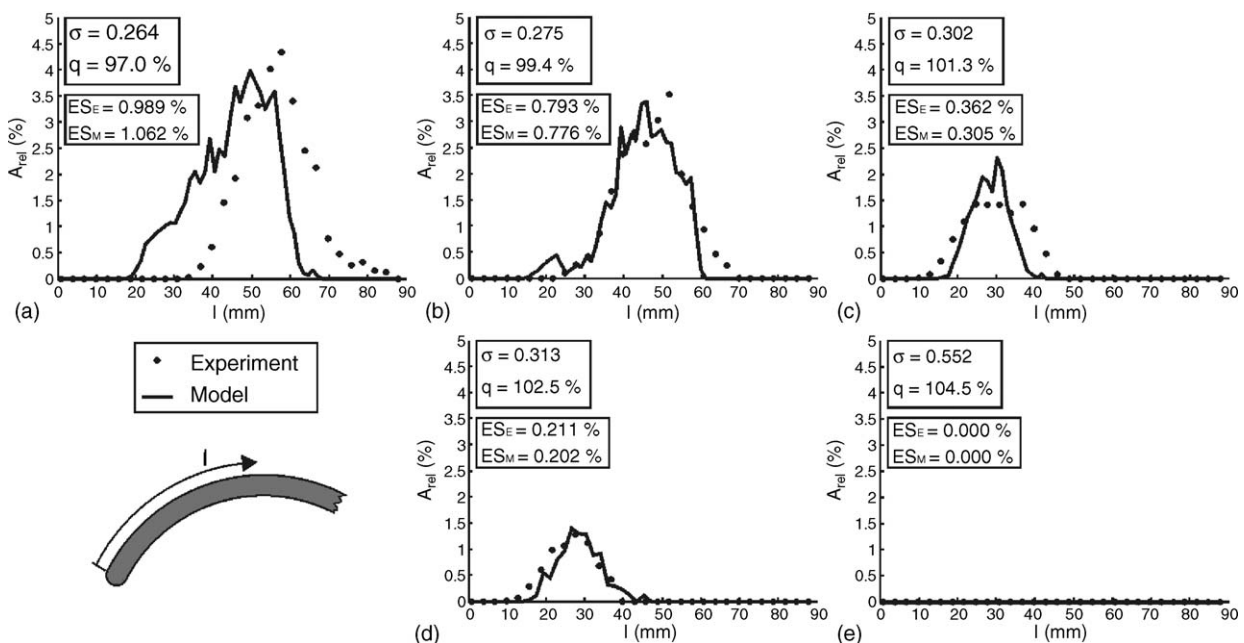


Fig. 20. Results of experimental measurements and model predictions of relative eroded surface as a function of distance from blade leading edge.

gas content was explained with the increase of attenuation of the pressure wave.

Conclusions derived from experimental results made it possible to develop a cavitation erosion model. The basic idea of the model is that a single pit is a result of a series of processes, which begins with a cavitation cloud separation and its collapse. At a collapse a shock wave is emitted. It spreads in the liquid and is attenuated by the distance as it travels from its source. Single bubbles that are positioned near the solid surface are influenced by the shock wave and can collapse in a form of a micro-jet, which hits the surface at a high velocity and creates the pit. The model uses data of visualization of cavitation structures as an input and predicts the magnitude and distribution of damage caused by cavitation erosion. It is also capable to reproduce the influences of flow velocity and water gas content. Since it uses little empiricism it is suitable for damage prediction on different geometries. To further test it, a prediction of cavitation erosion on a radial pump impeller was performed. The results of predictions were in a good agreement to the experimental data, especially regarding that only the visual information from the side view was used as an input to the model.

The presented model promises a good possibility of prediction and control of damage caused by cavitation erosion in real hydraulic machines.

References

- [1] F. Pereira, F. Avellan, Ph. Dupont, Prediction of cavitation erosion: an energy approach, *J. Fluids Eng.* 120 (1998) 719–727.
- [2] R. Fortes-Patella, J.L. Reboud, L. Briancon-Marjollet, A phenomenological and numerical model for scaling the flow aggressiveness in cavitation erosion, *Workshop on Cavitation Erosion, Bassin d'essais des carenes, Val de Reuil, France, 2004.*
- [3] M. Dular, B. Bachert, B. Stoffel, B. Sirok, Relationship between cavitation structures and cavitation damage, *Wear* 257 (2004) 1176–1184.
- [4] B. Sirok, M. Dular, M. Novak, M. Hocevar, B. Stoffel, G. Ludwig, B. Bachert, The influence of cavitation structures on the erosion of a symmetrical hydrofoil in a cavitation tunnel, *J. Mech. Eng.* 48 (7) (2002) 368–378.
- [5] M.S. Plesset, R.B. Chapman, Collapse of an initially spherical vapour cavity in the neighbourhood of a solid boundary, *J. Fluid Mech.* 47 (1971) 283–290.
- [6] W. Lauterborn, H. Bolle, Experimental investigations of cavitation-bubble collapse in the neighbourhood of a solid boundary, *J. Fluid Mech.* 72 (1975) 391–399.
- [7] M. Shimada, T. Kobayashi, Y. Matsumoto, Dynamics of cloud cavitation and cavitation erosion, in: *Proceedings of the ASME/JSME Fluids Engineering Division Summer Meeting, San Francisco, CA, 1999.*
- [8] C.E. Brennen, *Cavitation and Bubble Dynamics*, Oxford University Press, New York, Oxford, 1995.
- [9] L.L. Beranek, *Acoustics*, Acoustical society of America, New York, 1996.
- [10] P.A. Lush, Impact of a liquid mass on a perfectly plastic solid, *J. Fluid Mech.* 135 (1983) 373–387.
- [11] M. Dular, B. Sirok, B. Stoffel, Influence of gas content in water and flow velocity on cavitation erosion aggressiveness, *J. Mech. Eng.*, 2005.
- [12] B. Bachert, G. Ludwig, B. Stoffel, B. Sirok, M. Novak, Experimental investigations concerning erosive aggressiveness of cavitation in a radial test pump with the aid of adhesive copper films, in: *Proceedings of the 5th International Symposium on Cavitation, Osaka, Japan, 2003.*
- [13] M. Hofmann, Ein Beitrag zur Verminderung des erosiven Potentials kavitierender Stömungen, PhD Thesis, Technische Universität Darmstadt, Darmstadt, 2001.
- [14] R. Fortes-Patella, J.L. Reboud, A. Archer, Cavitation damage measurement by 3D laser profilometry, *Wear* 246 (2000).
- [15] J.L. Reboud, R. Fortes-Patella, A. Archer, Analysis of damaged surfaces. Part I. Cavitation mark measurements by 3D laser profilometry, in: *Proceedings of the 3rd ASME/JSME Joint Fluids Engineering Conference, San Francisco, CA, 1999.*
- [16] R.T. Knapp, J.W. Daily, F.G. Hammitt, *Cavitation*, McGraw-Hill Book Company, London, 1970.
- [17] R. Böhm, Erfassung und hydrodynamische Beeinflussung fortgeschrittener Kavitationszustände und ihrer Aggressivität, PhD Thesis, Technische Universität Darmstadt, Darmstadt, 1998.
- [18] H. Lohrberg, Messung und aktive Kontrolle der erosiven Aggressivität der Kavitation in Turbomaschinen, PhD Thesis, Technische Universität Darmstadt, Darmstadt, 2001.
- [19] B. Stutz, J.L. Reboud, Measurements within unsteady cavitation, *Exp. Fluids* 29 (2000).